fibers

MDPI

Article

Waste Bombyx Mori Silk Textiles as Efficient and Reuseable Bio-Adsorbents for Methylene Blue Dye Removal and Oil–Water Separation

Hansadi Jayamaha [1], Isabel Schorn [1] and Larissa M. Shepherd [1,*]

Department of Human Centered Design, Cornell University, Ithaca, NY 14853, USA; chj38@cornell.edu (H.J.); irs28@cornell.edu (I.S.)

* Correspondence: larissa.shepherd@cornell.edu; Tel.: (+1)-607-255-4288

Abstract: Many adsorbent materials are being studied for dye and oil removal from the environment. Bio-based materials such as silk are promising candidates due to their enhanced affinity for dyes and intrinsic hydrophobicity. This work extensively studies various silk textiles as dye and oil adsorbents. For comparison, we use electrospun fiber mats and hollow silk microparticle-treated silk fabrics. Our work is motivated by two factors: (i) massive amounts of silk waste is being discarded annually from textile factories, and (ii) the limited studies on the adsorption phenomena of pristine silk textiles. Based on our findings, 12 mg of silk filament yarn has a 90% methylene blue (MB) removal efficiency within 10 min of exposure for concentrations up to 100 ppm and exhibits adsorption capacities of 145 mg/g for 800 ppm concentrations. The adsorption kinetics obey a pseudo-second order, where the rate-controlling step is chemisorption, and isotherms follow the Langmuir model with homogenous monolayer adsorption. Furthermore, noil woven fabrics with contact angles of 140^0 have oil adsorbent capacities that are double the fabric weight. Our work confirms that silk waste textiles are efficient and reusable bio-adsorbents for MB dye and oil removal, outperforming materials made with additional and energy-intensive techniques such as silk dissolution and electrospinning.

Keywords: silk; textile waste; methylene blue removal; oil removal; adsorption mechanisms

Citation: Jayamaha, H.; Schorn, I.; Shepherd, L.M. Waste Bombyx Mori Silk Textiles as Efficient and Reuseable Bio-Adsorbents for Methylene Blue Dye Removal and Oil–Water Separation. *Fibers* **2024**, *12*, 99. https://doi.org/10.3390/fib12110099

Academic Editor: Damien Soulat

Received: 27 September 2024
Revised: 29 October 2024
Accepted: 7 November 2024
Published: 14 November 2024

1. Introduction

A variety of contaminants are continuously being released into waterways. Dye waste, particularly from the textile industry, causes agricultural land infertility, water scarcity, and other environmental issues [1]. Oil is also a pollutant, with an estimate of over 100 million gallons of crude oil entering oceans each year [2]. To address these concerns, water purification techniques such as the use of advanced dye- and oil-absorbent materials have become a critical area of research. Compared to traditional water purification methods (e.g., in situ burning, use of chemical dispersants, chemical solidification, and biological methods), these materials offer the potential to efficiently recover oil, adsorb contaminants, reduce secondary pollution, and allow for scalability at a low cost [1,3].

Unfortunately, the commonly used effective materials are synthetic and non-biodegradable, thus posing end-of-life disposal issues [4,5]. Such environmental concerns have fueled research on natural/biobased materials, such as the one studied here, silk. Silk is a biodegradable and biocompatible material obtained mostly from the cocoons of domesticated silk moths (*Bombyx mori*). Comprehensive reviews are available detailing water purification using various silk-based materials including aerogels, nanofibers, silk fibroin-coated nanoparticles, poly tetrafluoro ethylene-treated silk fabrics, etc. [4–6]. Despite the potentially positive environmental impact of using silk and the possibility of sourcing from the textile industry's discarded materials, most reported work involves reprocessing of silk with lengthy dissolution times, multiple hazardous chemicals, and/or energy-intensive techniques [1,4,6–10].

Our study investigates the use of silk textile remnants as a material for decontaminating water sources, without reprocessing the silk material using lengthy and energy-intensive methods. We study pristine silk fabrics with various fabric and yarn structures, as well as dyed silk fabrics, to show their potential application for both dye and oil removal. The results are then compared with regenerated electrospun silk, degummed natural silk fibers, and fabrics treated with hydrophilic hollow silk microparticles to confirm the intrinsic adsorption capacity of pristine silk waste textiles.

For dye adsorption studies, we chose a cationic dye, methylene blue (MB), as it is a commonly used industrial dye that has potential risks of mutagenic and carcinogenic effects and bioaccumulation even at very low concentrations [1]. These adsorption studies are carried out using periodic absorbance measurements of dye solutions exposed to silk textiles. The absorbance readings of the solutions are taken using a UV–visible spectrometer. To study the oil adsorbent properties, we use commercially available oil (i.e., gasoline and corn oil) and measure the oil uptake per unit weight of textile using a laboratory scale. We verify the reusability of the silk adsorbents for over 10 cycles. As mentioned by Mehdi et al. in a recent publication, ethanol is used for MB desorption [11], and oil is mechanically pressed out to regenerate the silk textile.

We find that unraveled silk fabrics (yarns) achieve more than 90% adsorption within 10 min for MB concentrations as high as 100 ppm. This removal efficiency is higher than those of electrospun fiber mats and natural silk fibers of equal weight. Similarly, promising results are observed for oil affinity; woven silk noil fabrics adsorb oil up to double the fabric's initial weight while retaining 50% of its capacity for over 10 cycles. Through this extensive study on adsorption efficiency, isotherms, and kinetics, we substantiate the potential of silk textile remnants as effective, efficient, and economical bio-adsorbents for MB dye and oil removal from aqueous solutions. Therefore, we introduce a potential use for silk textile waste as a bio adsorbent and confirm that no additional processing is required for its use as an MB and oil remover.

2. Materials and Methods

2.1. Materials

All fabrics and yarns were from domesticated *B. mori* silk. Silk broadcloth was purchased from Testfabric Inc., West Pittston, PA, USA. For the synthesis of hollow silk microparticles (SPs) and the electrospinning of silk fibers (ESs), analytical-grade 1,1,1,3,3,3-hexafluoroisopropanol (HFIP) ($\geq$ 99% purity) was purchased from Sigma Aldrich, and degummed *B. Mori* silk fibers (SFs; with sericin protein removed) were purchased from Woolery Inc., Arlington, OR, USA. The dialysis tubes (MWCO 3.5 kD) used in the synthesis of hollow SP were purchased from Spectrum Labs Inc., San Francisco CA, USA. The methylene blue hydrate (MB) used in dye absorption studies was also purchased from Sigma Aldrich. Pure ethanol from Koptec was used to test the reusability of the fabrics. Corn oil and gasoline were purchased from the general store. All reagents were used as received, without further purification.

2.2. Hollow Silk Particle Synthesis and Fabric Treatment

Degummed silk cocoon fibers (1 g) were soaked with 16 mL of HFIP in a sealed 20 mL glass container for 24 h at 40 °C in an oven (Fisher Scientific Isotemp, Newington, NH, USA), followed by stirring on a hotplate (Thermo Scientific, Waltham, MA, USA) for another 48 h at 40 °C. After cooling, the uniformly dissolved solution was dialyzed in parts against water for 3 days, changing the water every 24 h. The undissolved fiber was collected at the bottom of the dialysis tube, and the remaining solution was decanted and filtered using 3-micron syringe filter tips (Celltreat, Pepperell, MA, USA) to obtain the silk particle solution. The particle solution was then stored at 4 °C for further studies. The solution (10 mL of 18% w/v solution) was poured/cast onto fabrics (5 $\times$ 5 cm^2) and allowed to dry at room temperature overnight at a humidity ~30%.

2.3. Electrospinning Silk Nanofiber Mats

Degummed silk cocoon fibers (1 g) were soaked with 16 mL of HFIP in a sealed 20 mL glass container for 24 h at 40 °C in an oven (Fisher Scientific Isotemp), followed by stirring on a hotplate (Thermo Scientific) for another 48 h at 40 °C. After cooling, the uniformly dissolved solution was electrospun using a traditional setup. A 1.5-inch-long, 20-gauge disposable nonbeveled needle (Nordson EFD LLC, Austintown, OH, USA) was fitted to a 5 mL glass syringe (Chemglass, Vineland, NJ, USA). The voltage was maintained at 15 kV (Gamma High Voltage Research Inc., Ormond Beach, FL, USA) A flow rate of 1 mL/h was then applied using a PH Ultra syringe pump (Harvard apparatus, Holliston, MA, USA). The solution was directly electrospun over a gap of 10 cm onto a copper stationary collector plate wrapped with an aluminum sheet.

2.4. Dye Adsorption Studies and Reuse Studies

A stock solution of MB (1000 mg of MB in 1000 mL of distilled water) was prepared and serially diluted to generate a series of concentrations from 1 to 100 ppm. The optical densities (absorbance) of each solution were measured using a UV–visible spectrophotometer (Shimadzu 2550, Shimadzu Scientific Instruments Inc., Columbia, MD, USA) at a 664 nm wavelength, corresponding to the maximum wavelength for MB [1]. We systematically constructed a linear plot consisting of MB concentrations ranging from 1 to 100 ppm to establish a linear calibration curve for MB.

The adsorbent (a variety of silk textiles with dimensions of 1.2 × 1.2 cm^2) was dipped in 5 mL MB solutions of a 10 ppm concentration. The efficiency of MB removal (%) by the adsorbent (5 mL MB solution/1.2 × 1.2 cm^2 textile substrate) was calculated at different time intervals with the following equation:

$$\text{MB removal efficiency (\%)} = (C_o - C_t)/C_o \times 100 \quad (1)$$

where C_o and C_t are the initial and residual concentrations of MB in the stock solution and filtrate, respectively.

The adsorption capacity (Q_e) of adsorbents was determined with the following equation for a range of concentrations from 5 to 800 ppm:

$$Q_e\ (mg/g) = (C_o - C_e) \times (V/W) \quad (2)$$

where C_o and C_e are the initial and the equilibrium concentrations of MB (mg/L), V is the volume of the MB solution (L), and W is the weight of the adsorbent (g). The maximum absorption capacity was also experimentally calculated at a concentration of 10 ppm for the PWY, NWY, PWY-T, and NWY-T samples by measuring the weight gained by the textiles exposed to 150 ppm MB solutions. We investigated the adsorption kinetics of the most efficient adsorbent (PWY) using pseudo-first and second-order models with the equations given below:

Pseudo-first-order model:

$$\log (Q_e - Q_t) = \log Q_e - k_1\ t/2.303 \quad (3)$$

Pseudo-second-order model:

$$T/Q_t = 1/(k_2\ Q_e^2) + t/Q_e \quad (4)$$

where Q_t and Q_e (mg/g) are the adsorption capacity at time t and equilibrium, respectively, and k_1 (min^{-1}) and k_2 (g/mg·min) are the first- and second-order rate constants, respectively. The equilibrium isotherms of the PWY sample were also studied using the Langmuir and Freundlich models.

Langmuir isotherm:

$$C_e/Q_e = 1/b\ Q_m + C_e/Q_m \quad (5)$$

Freundlich isotherm:

$$\log Q_e = \log K_F + (1/n) \log C_e \quad (6)$$

where Q_e is the equilibrium adsorption capacity of the MB adsorbed onto the adsorbent (mg/g), C_e is the equilibrium concentration of MB (mg/L), and Q_m and b are Langmuir constants associated with the maximum adsorption capacity and binding energy, respectively. K_F and n are empirical constants, where the former is known as the Freundlich constant (L/mg) and the latter as the heterogeneity factor. The separation factor (R_L), which indicates whether the adsorption phenomena are favorable, can be calculated using the below equation:

$$R_L = 1/(1 + K_L \cdot C_0) \quad (7)$$

where K_L is the Langmuir constant (L/mol), and C_0 is the initial adsorbate concentration (mol/L).

To test the reusability of the PWY samples, ethanol was used to desorb the MB dye as per the literature [11]. The adsorption and desorption efficiencies were measured for 10 cycles. We repeated all experiments twice.

2.5. Oil Adsorbent and Reuse Studies

The level of hydrophobicity of the fabrics was measured using a Rame-Hart 500 contact angle goniometer. The contact angle was recorded over a duration of 5 min for each sample. The oil absorbent capacity was calculated using Equation (8). The oil–water mixtures were prepared by dispersing oil (50 mL) in water (200 mL) with stir plate agitation until an oil-in-water emulsion-like mixture was formed.

$$\text{Oil adsorption capacity (g/g)} = (w - w_0)/w_0 \quad (8)$$

where w_0 is the initial weight and w is the final weight after allowing excess oil to drip off. The reusability was assessed by mechanically pressing the fabric to remove the oil and remeasuring the oil adsorbent capacity. Each measurement was taken three times, and the average value was recorded.

2.6. Characterization of Hollow Silk Particles and Treated and Pristine Fabrics

The morphology and size distribution of the hollow silk particles and electrospun fiber mats were analyzed using the Zeiss Gemini 500 FE-SEM (Zeiss, Oberkochen, Germany). Particles dried on an aluminum stub were sputter-coated with gold palladium for 40 s before imaging at an accelerating voltage of 1 kV. The fabrics (pristine and treated) and electrospun fiber mats were attached to aluminum stubs and sputter-coated and viewed under the FE-SEM using the same parameters. We measured the diameter of the silk particles using ImageJ.JS v0.5.8 software. An average value of 50 measurements was taken. The microstructure of the silk yarns was also studied using the light microscope (Olympus BX51, Olympus Life Science, Westborough, MA, USA). The secondary protein conformational content was quantified for natural silk fibers (degummed), silk dope, silk particles, and the PW fabric using the PerkinElmer Fourier Transform Infra-Red (FTIR) spectrophotometer (PerkinElmer, Waltham, MA, USA) in the range of $4000-600\ cm^{-1}$. The second derivative of the amide I band was deconvoluted and curve-fitted to obtain the sub-spectra for each of the secondary conformations. The percentage of the area occupied by each sub-spectrum was then calculated to quantitatively obtain the content (%) of each secondary structure for SF, SFS, PW, and SP.

3. Results

3.1. Conformational Analysis of Silk Textiles from FTIR Spectra

Silk textiles are available in many forms—natural silk fibers, fabrics, yarns, and regenerated micro/nanofibers. For the current study, different fabric and yarn structures

were considered (Table 1 and Figure 1A–F). Plain woven (PW) silk fabrics composed of (i) filament yarns and (ii) noil woven (NW) fabrics consisting of short fibers spun into yarns were used due to their different surface textures and morphologies. Figure 1A,B portray the increased macro-level roughness of the NW compared to PW fabrics. Figure S1 also provides the micro-level structure of the yarns—PW yarns have smooth and continuous filaments, while NW yarns have a short protruding, "hairy" assembly of fibers. Therefore, NW yarns have a higher surface roughness than PW yarns.

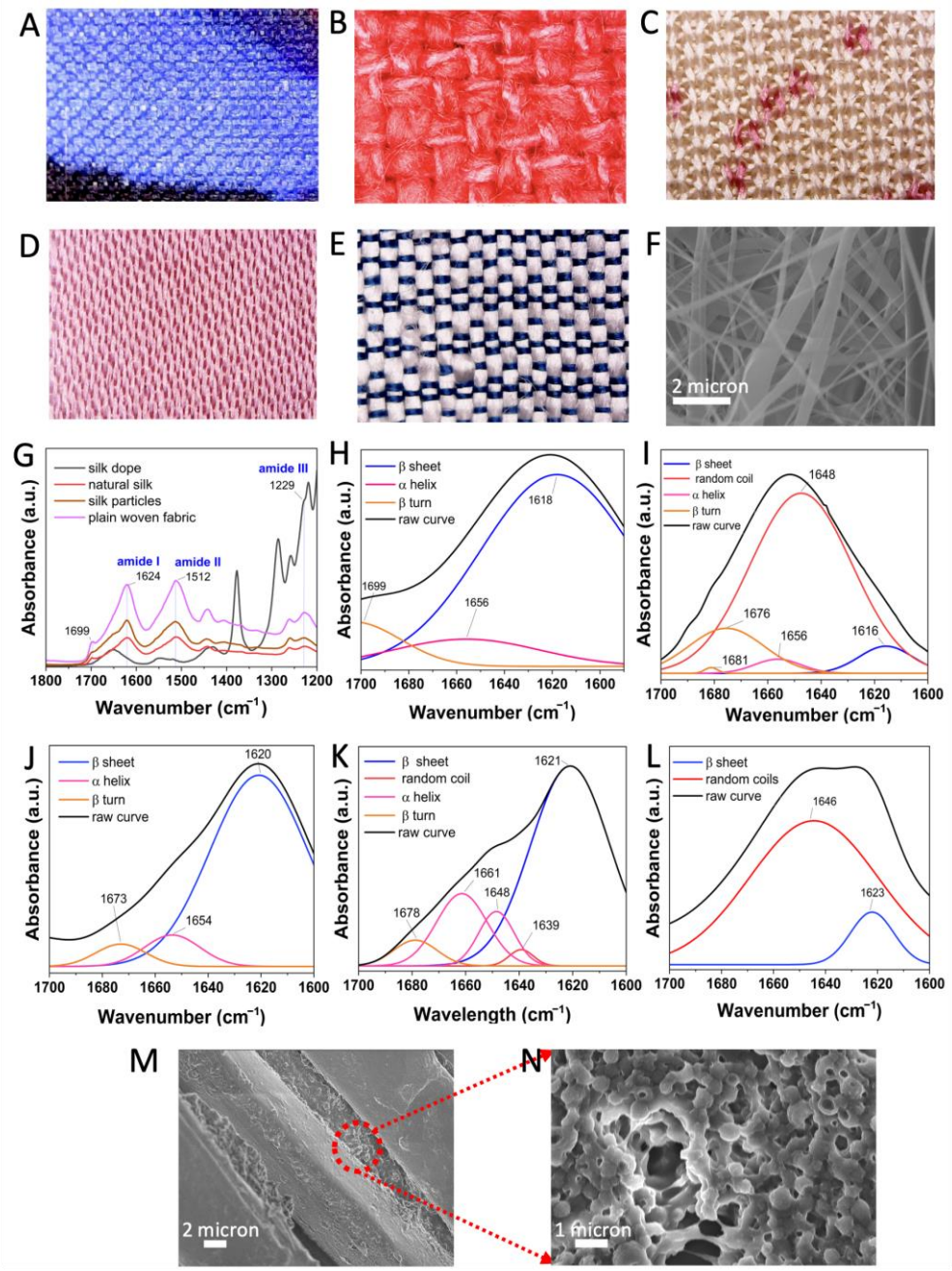

Figure 1. Conventional silk textiles: (**A**) plain woven dyed fabric, PW-D; (**B**) noil woven dyed fabric, NW-D; (**C**) dyed single Jersey knit fabric, JK-D; (**D**) dyed Satin (Charmeuse) woven fabric, CW-D; and (**E**) dyed Shantung (Duponi) woven fabric, SW-D. (**F**) SEM image of electrospun fiber mat; (**G**) FTIR spectra depicting amide bands I, II, III for silk dope or silk fibroin solutions, SFS; natural silk fiber, SF; silk particles, SPs; and PW fabric. FTIR sub spectra of (**H**) SF, (**I**) SFS, (**J**) PW, (**K**) SP, and (**L**) ES and SEM images of (**M**) treated PW fabric, PW-T, and (**N**) SP.

Table 1. Various forms of silk textiles used for methylene blue dye adsorption studies.

	Description	Yarn Type	Annotation	Grams/Meter^2 (GSM)
1	Plain woven fabric	filament	PW	88
2	Plain woven fabric—treated	filament	PW-T	88
3	Plain woven fabric—dyed	filament	PW-D	34
4	Noil woven fabric	spun yarn	NW	135
5	Noil woven fabric—treated	spun yarn	NW-T	135
6	Noil woven fabric—dyed	spun yarn	NW-D	176
7	Dyed Shantung (Duponi) fabric	filament and spun-slub yarn	SW-D	100
8	Dyed Satin (Charmeuse) fabric	filament	CW-D	80
9	Dyed silk Jersey knit fabric	filament	JK-D	142
10	Electrospun fiber mats	nanofibers	ES	9
11	Natural silk fibers	natural fibers	SF	-
12	Unraveled Noil fabric	filament and spun yarn	NWY	-
13	Unraveled Plain fabric	filament	PWY	-
14	Unraveled Noil fabric—treated	filament and spun yarn	NWY-T	-
15	Unraveled Plain fabric—treated	filament	PWY-T	-
16	Unraveled Plain woven dyed fabric	filament	PW-DY	-

Silk proteins are amphiphilic in nature with large hydrophobic domains occupying the major component of the polymer, which has a high molecular weight [12]. The hydrophilicity is due to the constituent glycine (Gly), alanine (Ala), and serine (Ser) amino acids. These form the heavy chains (~390 kDa) with a repetitive hexapeptide sequence of Gly-Ala-Gly-Ala-Gly-Ser and repeats of Gly-Ala/Ser/Tyr dipeptides, which can form stable anti-parallel β-sheet crystallites. The light chains (~26 kDa) are nonrepetitive and form the hydrophilic and more elastic section of the peptide [13–15].

Figure 1G presents the FTIR spectra displaying the amide I, II, and III absorption bands, which represent the three crystalline forms—silk II with an anti-parallel β-sheet structure [16], silk I with a metastable state between the α-helix and β-sheet structures [17], and silk III for a form of air–liquid interfaces [18]. Table S1 presents the FTIR absorbance bands of β-sheet, α-helix, and random coils as per the literature [19,20]. The amide I region is often deconvoluted in quantitative analysis of the secondary conformation content [21]. Figure 1H–L and Table 2 provide the sub-spectra for each secondary conformation and the percentage content, respectively, for the silk fiber (SF), silk fibroin solution (SFS), PW, and silk particles (SPs). The significantly higher β-sheet conformations (~80%), as apparent from the sub-spectra of Figure 1I,K, and Table 2, confirm that the SF and PW fabrics are predominantly hydrophobic.

Table 2. Content of secondary protein structural conformations in PW, SF, SFS, SP, and ES.

Sample	β Sheets (%)	Random Coils (%)	α Helices (%)	β Turns (%)
PW	80.9	-	13.6	5.55
SF	79.2	-	10.7	4.77
SF solution (SFS)	5.84	77.2	2.81	14.1
SP	67.3	1.81	25.8	5.13
ES	10.7	89.3	-	0.0206

Secondary protein conformations can be restructured by dissolving the SF and reassembling the solution to form SPs; therefore, we use FTIR data to understand the effect of the synthesis steps on the secondary protein conformations. The synthesis route, similar to an emulsion method, results in hollow microparticles with outer diameters of 577 ± 96 nm (Figure 1M,N). Figure S2 schematically represents the synthesis steps. In the silk solution (silk fibroins in1,1,1,3,3,3- hexafluro-2-propanol, HFIP, which we refer to as SFS), the HFIP molecules tend to cluster around the polypeptide chains, forming a coating and amplifying the local tendency of the silk fibroin to form a preferred secondary conformation like a random coil structure, which is confirmed by a significantly higher content (~77%) of random coils in the SFS (Figure 1I and Table 2). During dialysis, the water–HFIP system behaves as an HFIP/water emulsion, allowing for the formation of hollow silk particles. The HFIP molecules are gradually stripped off the surface of the silk particles, resulting in the unfolding of the random coils and the formation of more stable α-helix and β-sheet conformations.

The alteration in the chemical environment results in distinct shifts of the characteristic amide bands of SFS (Figure 1J) to higher wavenumbers relative to the peak positions of the SF and SP. A relatively higher amount of α-helix (25.8%) can be observed in the SP compared to the α-helix content (10.7%) in the SF (Figure 1H,K), resulting in the lesser crystallinity and higher dye penetrability of the SP. Although the amount of β-sheet in the SP is reduced, a significant amount remains (67.3%), leading to some hydrophobicity. In contrast, the electrospun fiber mats (ES) fabricated from the same SFS have primarily random coils (89.3%) and significantly lower amounts of β-sheet (10.7%), resulting in predominantly amorphous materials with hydrophilicity (Figure 1L). The authors attribute this to the rapid solidification of the fibers during electrospinning, resulting in an inadequate amount of time for the restructuring of the random coils to more stable conformations.

3.2. Dye Adsorption Studies of Pristine and Treated Silk Textiles

We studied the adsorption properties of the textiles and unraveled textiles (yarns) given in Table 3 towards MB solutions of concentration 10 ppm. To ascertain the use of cut waste silk fabrics from the industry for water treatment, we selected a few other fabric structures and dyed fabrics with various fabric and yarn constructions and studied their dye adsorption properties. MB molecules are planar, aromatic, and cationic in nature and result in stacking on the substrate through hydrogen bonding and coulombic interactions [1,22]. Silk fibroins are predominantly anionic in nature due to constituent Gly, Ala, and Ser amino acids, which make up 85% of the protein in silk and enable the adsorption of MB dye molecules [7,23]. The PW and NW fabrics are treated with the hollow SP to increase the specific surface area and the hydrophilicity of the fabrics due to the particle morphology (hollow spheres) and reduced β-sheet content of SP, as summarized in Table 2. Table 3 presents the removal efficiency at 30 min and the total time taken for more than 90% of MB adsorption. The treated fabrics (PW-T and NW-T) are more efficient at MB removal than their pristine counterparts and have higher adsorption capacities (Table S2). This substantiates that both the silk protein conformation and surface morphology are crucial parameters for optimum adsorption phenomena.

Although the dyed fabric adsorption is marginally lower than that of the PW and NW fabrics, the removal efficiency of dyed fabrics is also nontrivial. The NW-D fabrics show almost similar adsorption efficiencies to PW-T fabrics during the first 30 min. Silk fabrics are generally dyed using acid dyes, which have anionic groups such as sulphonates [24]. The anionic dyes enhance the ionic density of the fabric, making it more hydrophilic. This explains the significant adsorption efficiency we see in dyed fabrics such as NW-D and PW-D. However, the dyed fabrics take a relatively longer time to reach equilibrium conditions (7+ hours for 90% dye adsorption) due to the lower concentration of unoccupied binding sites on dyed silk fabrics (due to the textile dye already occupying potential binding sites).

Table 3. Removal efficiencies in 10 ppm MB solution of various silk textiles and yarns.

Sample	Adsorption at 30 min (%)	Complete Adsorption (>90.0%) (minutes)
PW	27.7	360
PW-T	39.4	360
NW	12.6	420
NW-T	32.6	420
PW-D	15.8	420+
NW-D	32.3	420+
SW-D	23.4	420+
CW-D	2.78	420+
JK-D	19.4	420+
PWY	96.9	1
PWY-T	94.1	3
NWY	92.9	1
NWY-T	92.8	5
PW-DY	87.8	40
ES	56.8	240
SF	91.0	30

By unraveling the fabric into their yarn form, a multifold increase in exposed surface area can be achieved. With this increase in surface area, the removal efficiency of the unraveled plain silk fabric (PWY) significantly increases, resulting in a more than 300× increase in removal rate compared to PW. For further comparison to what is commonly researched, we electrospun ES nanofiber mats (225 ± 177 nm) and carried out adsorption studies using equal weights of ES (Figure 1G) as PW fabrics. Interestingly, all unraveled fabrics, or in other terms, yarns (PWY, NWY, PWY-T, NWY-T), as well as the SF, achieve a more rapid adsorption of the dye compared to ES. As explained in the previous section, ES predominantly comprises random coil domains, which results in its hydrophilicity, and being that it is a nanofiber mat, it has a high specific surface area. Therefore, it is unclear why unraveled silk textiles outperform the ES mats. We hypothesize that the underlying reason(s) may be the result of the modified surface chemistry of the fibers due to residual solvents in ES fibers and/or the less accessible structure of the fiber mats.

Similar to the behavior we observe for PW-D and NW-D fabrics, unraveled dyed fabrics (PW-DY) show a >90% dye adsorption within 40 min (Table 3). Although the removal efficiency is marginally lower due to the limited number of unoccupied binding sites, it is still comparable to undyed PWY and NWY and significantly better than PW and NW fabrics. These results demonstrate that additional energy-intensive techniques such as silk dissolution and electrospinning are not required for MB removal and, instead, the remnants of silk textiles can be used as more efficient silk-based adsorbents.

3.3. Adsorption Kinetics, Equilibrium Isotherms, and Reusability Studies of PWY

As mentioned previously, the PWY sample showed rapid adsorption of MB, even faster than the ES mat of equal weight. Therefore, for the subsequent adsorption kinetic and equilibrium studies, the sample PWY was used with an initial MB concentration of 10 mg/L. We studied the removal efficiency (%) over time (Figures 2A and S4 and Table S3). A significantly faster adsorption process was observed within the first minute due to the existence of a large number of active adsorption sites. Notably, in the first 3 min, ~95% of MB was removed from the solution. The adsorptions reached saturation by 30 min, which was chosen as the equilibration time for the subsequent tests. At this stage, the

removal efficiency reached ~97%. Kinetic studies provide critical information on the rate of adsorption processes [25]. The pseudo-first-order and pseudo-second-order models were applied to investigate the adsorption kinetics behavior of the PWY. Figure 2B,C and Table 4 present the plots and summarize the kinetic adsorption parameters calculated from these two models. The adsorption process of MB is better represented by the pseudo-second-order model, as apparent from the higher correlation coefficient (R^2) of 0.999. Therefore, the adsorption type is chemisorption, meaning that chemical interactions are in effect during the adsorption process. MB dissociates into cationic MB and anionic chloride ions when dissolved in water. The cationic MB molecules interact with functional groups that are present in silk protein forming a silk–dye complex via electrostatic interactions and hydrogen bonding with the protonated amino group [6,26]. Chemisorption is further confirmed by FTIR with the appearance of a peak 1330 cm^{-1} after MB adsorption. The peak at 1330 cm^{-1} is attributed to the (–OH) bending of phenolic groups, indicating bond formation between the dye and silk's functional groups (Figure S3). These results show that silk-based adsorbents undergo chemisorption and are in line with the previous literature discussing the use of silk cocoons and silk natural fibers as adsorbents [7,23].

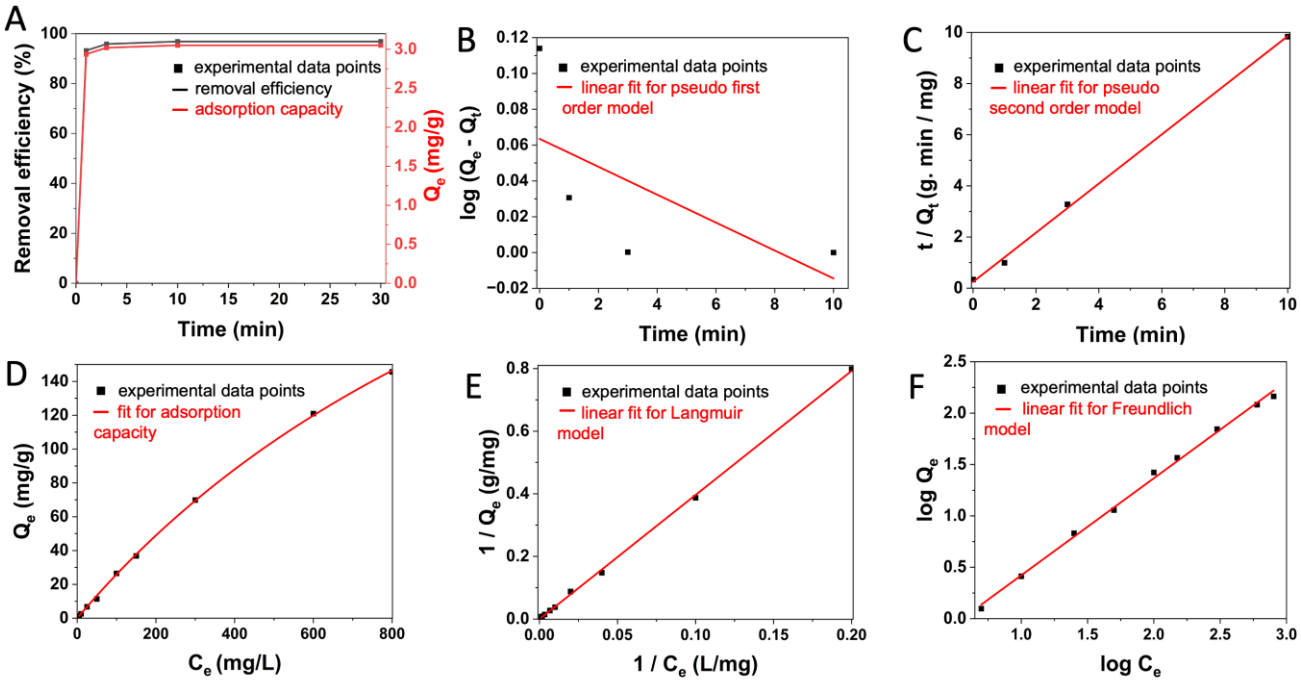

Figure 2. (**A**) Removal efficiency and adsorption capacity of PWY plotted against time, (**B**) pseudo-first-order model and linear plot for dye removal by PWY, (**C**) pseudo-second-order model and linear plot for dye removal by PWY, (**D**) adsorption capacity versus MB concentration plot for PWY and nonlinear fitting using Langmuir model, (**E**) linear plot for PWY using Langmuir model, and (**F**) linear plot for PWY using Freundlich model.

Table 4. Kinetic parameters for the adsorption of MB (10 ppm) by PWY from pseudo-first-order and -second-order models.

Experimental	Pseudo-First-Order Model			Pseudo-Second-Order Model		
Q_e (mg/g)	Q_e (mg/g)	K_1 (min^{-1})	R^2	Q_e (mg/g)	K_2 ($g.mg^{-1}.min^{-1}$)	R^2
2.96	1.16	−0.0180	0.427	1.04	3.71	0.999

From the linear fitting, the equilibrium adsorption capacity (Q_e) was calculated to be 1.04 mg/g, which is correlated with the experimental adsorption capacity (Q_{exp}) of 2.96 mg/g. It should be noted, however, that the adsorption capacity depends on the initial

concentration of the MB solution, and the adsorption capacity of PWY can reach as high as 140 mg/g for an initial MB concentration of 800 ppm.

The adsorption equilibrium was characterized using adsorption isotherms by altering the adsorbate concentration from 5 to 800 ppm. Here, the adsorption results were fitted with two well-known models, the Langmuir and Freundlich models, to evaluate the equilibrium isotherms [27]. The Langmuir isotherm represents an attempt to model the adsorption assuming the adsorbent has a limited number of identical (homogeneous) adsorptive sites and undergoes monolayer adsorption. The Freundlich model represents an adsorption model that assumes that the adsorbent has nonuniform (heterogeneous) adsorptive sites and undergoes multilayer adsorption [27–29].

Figure 2D indicates that the adsorption is nonlinear with a finite number of adsorption sites. The resulting equilibrium parameters are summarized in Table 5, and the plots are displayed in Figure 2E,F and Figure S5A,B. The R^2 values for the linear fitting of the two models are similar, with the Langmuir model fitting marginally better (R^2 = 0.999) compared to the Freundlich model (R^2 = 0.997). Based on previous research [7], and based on our results, we conclude that the applicable adsorption phenomena is the homogenous monolayer adsorption of dye molecules with a relatively high adsorption capacity (Q_m) of 436 mg/g and Langmuir constant of 6.32×10^{-4}. Gupta et al., who reported that silk natural fibers undergo homogeneous monolayer adsorption, have performed adsorption experiments for adsorbate concentrations up to 100 ppm [7]. In our study, due to the linear nature of the adsorption plot in the range 5–150 ppm (Figures 2D and S6; suggesting infinite adsorption), the concentration range is widened up to 800 ppm for a better representation of the finite adsorption process. The favorability of the adsorption process can also be further analyzed using the separation factor, R_L. The value of R_L in the range of 0–1 suggests that the adsorption process is favorable, and an R_L higher than 1 suggests that the process is unfavorable. For PWY, R_L is calculated to be 0.999, indicating that the adsorption is favorable (Table S4).

Table 5. Langmuir and Freundlich isotherm model parameters for the adsorption of MB (5–800 ppm) by PWY.

Langmuir Isotherm			Freundlich Isotherm		
Q_m (mg/g)	B (L/mg)	R^2	n	K_F	R^2
436	6.32×10^{-4}	0.999	1.22	0.611	0.997

The removal efficiencies and visual change in dye concentration (or color) for MB concentrations of 5–800 ppm are provided in Table S5 and Figure 3A. PWY has removal efficiencies of 98.0% up to 150 ppm and 71.4% even at 800 ppm. In terms of the removal efficiency and time taken for equilibrium adsorption, pristine PWY has significant promise compared to other silk-based adsorbents, which require additional preparation that involves energy-intensive and time-consuming processes [1,4,6–11]. Table S6 provides adsorption capacities of other silk-based materials for MB dye removal. The authors also direct the readers to a review article, which summarizes silk composite materials for water treatment [6]. These findings show that significantly higher adsorption capacities can be achieved by functionalizing silk composites using sophisticated methods and costly nanomaterials; however, our study confirms that waste silk material, that is, silk without any additional processing, can also achieve high adsorption capacities.

Due to the high adsorption capacities, the unraveled fabric can be reused (multiple adsorption–desorption cycles) for MB solutions of an initial concentration of 10 ppm (Figure 3B,C and Table S7). As per the literature [11], we observed that the MB dye can be desorbed into ethanol while mechanically shaking using a wrist action shaker. PWY continues to have removal efficiencies of over 90.0% for 10 cycles. However, on average, only 30.1% of the adsorbed MB is desorbed by mechanically shaking in ethanol for 3 h.

After every four cycles, the concentration of desorbed MB increases as a result of the cumulative amount of MB dye remaining attached to the adsorbent.

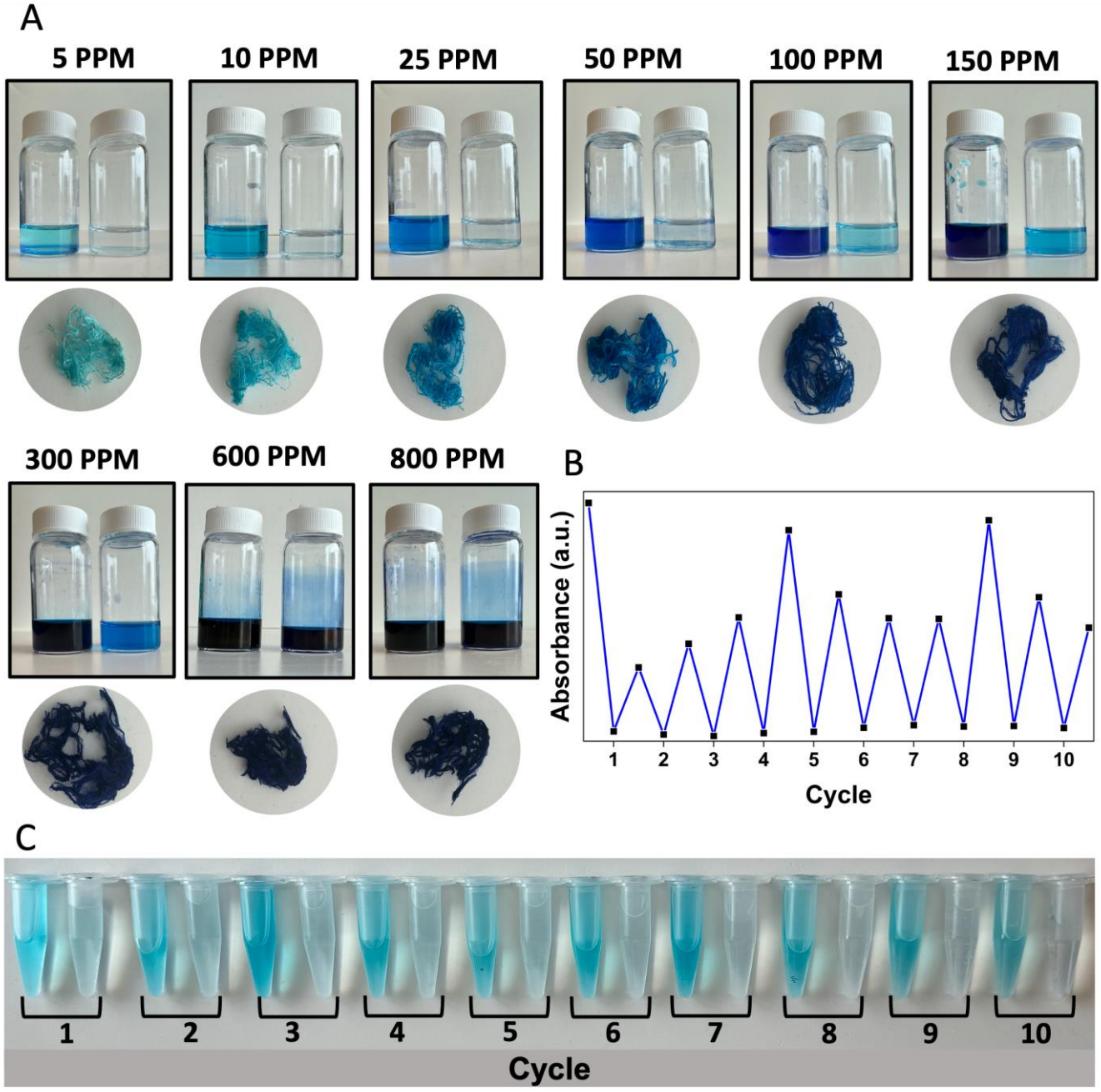

Figure 3. (**A**) Visual representation of color changes at equilibrium dye removal of both MB solutions and PWY samples at increasing MB concentrations from 5 - 800 ppm, (**B**) graphical representation of the adsorption-desorption cycles of MB dye removal by PWY (up to 10 cycles), and (**C**) visual representation of the adsorption-desorption cycles of MB dye removal by PWY (up to 10 cycles).

3.4. Oil–Water Separation by Pristine and Treated Silk Textiles

The literature mentions various functionalized silk textiles as oil separators [3,4]. As discussed in previous sections, silk textiles possess intrinsic hydrophobicity due to the significant content of β-sheet crystallite structures and are therefore suitable as oil adsorbents, while the dyed silk fabrics are hydrophilic due to the surface charges from the anionic dyes used, making them ineffective oil adsorbents. The hydrophobic/hydrophilic nature of silk textiles is quantified by contact angle measurements (Table 6). The undyed

fabrics (PW and NW) and their treated counterparts (using hollow silk particles) have contact angles of ~140^0 (Table 6, Figure 4A,B).

Table 6. Contact angle measurements for silk textiles (measurements are taken after 5 min of ejecting 200 µL of distilled water onto the fabric surface).

Sample	CA After 5 min (Degrees)
PW	139 ± 2
PW-T	140 ± 1
PW-D	0
NW	142 ± 2
NW-T	140 ± 2
NW-D	0
ES	0
SW-D	0
CW-D	0
JK-D	0
HW-D	0
SP	0

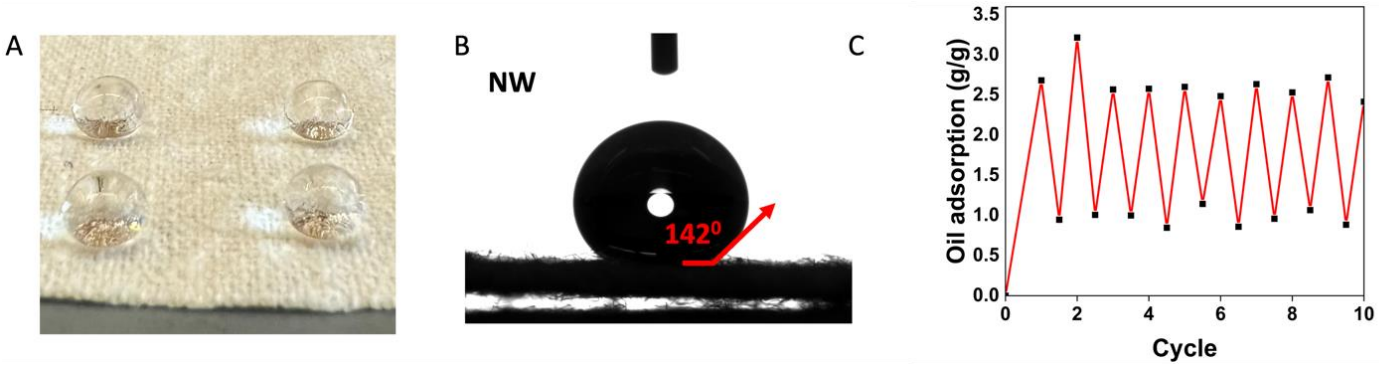

Figure 4. (**A**) Visual representation of water droplets on NW fabrics, (**B**) contact angle measurement for NW fabric, and (**C**) corn oil adsorption of NW fabric during 10 cycles of repeated adsorption and desorption.

Due to their high contact angles, PW, NW, and their treated fabrics were dipped in oil–water solutions (25% v/v oil solutions), and the oil weight gain was measured. Due to the higher surface roughness and specific surface area of the NW and NW-T fabrics, they show oil capacities three times the initial weight of the fabric for the adsorption of corn oil and close to twice the weight for the adsorption of gasoline (Table 7). We also highlight the fact that the fabrics can be used repeatedly for over 10 cycles (Figure 4C). Promisingly, the capacity does not decrease any further after the initial drop in the first cycle and remains at approximately 1g/g over an additional nine adsorption–desorption cycles. Based on these measurements, we highlight the possibility of using pristine silk fabrics as oil–water separators, without requiring any additional sophisticated treatments.

Table 7. Adsorption capacity of different silk textiles for gasoline and corn oil.

Sample	PW	PW-T	NW	NW-T
Corn Oil Capacity (g/g)	2.19 (±0.39)	2.01 (±0.16)	3.28 (±0.08)	3.21 (±0.37)
Gasoline Capacity (g/g)	0.829 (±0.063)	0.862 (±0.214)	1.92 (±0.12)	1.47 (±0.08)

4. Conclusions

This study confirms that waste silk fabrics can be used as an effective, efficient, and reusable MB dye and oil removal material, thus providing an opportunity to repurpose a substantial waste source from the textile industry. While beyond the scope of this work, we believe that future studies on (i) fiber shedding during the adsorption process and (ii) the effect of various fabric pretreatments on the adsorption capacity would allow for further understanding of the full use potential of waste silk textiles and yarns. In this work, we studied various silk fabrics and yarns to quantify their dye removal efficiencies. Although already-dyed fabrics show marginally lower removal efficiencies, all fabrics chosen for the study show potential for MB dye removal. Unraveled fabrics (PWY and NWY), the silk yarns, have significantly faster adsorption rates and capacities due to a higher exposed surface area. Their removal efficiency is even higher than electrospun fiber mats of equal weight. As a result, we chose PWY for further adsorption studies. Based on the findings, 12 mg of PWY have a 90% removal efficiency within 10 min of exposure to 5 mL of MB solution of up to 100 ppm concentrations. Additionally, PWY exhibits large equilibrium adsorption capacities of 145 mg/g for 800 ppm MB concentrations. The kinetics of adsorption obey the pseudo-second-order model, indicating that the rate-controlling step is chemisorption, and the data have the best fit to the Langmuir isotherm exhibiting homogenous monolayer adsorption. Not only are silk textiles biodegradable and biocompatible [17,30], but we confirm that the textiles can be repeatedly used over 10 adsorption–desorption cycles. Furthermore, NW fabrics demonstrate contact angles of 140^0 and have oil adsorbent capacities of double the fabric weight and the ability to be reused over 10 cycles, with the oil adsorption capacity reducing only after the first cycle. In conclusion, this study substantiates the possibility of using silk waste as an efficient and reusable adsorbent for MB dye and oil removal from aqueous systems.

Supplementary Materials: The following supporting information can be downloaded at: https://www.mdpi.com/article/10.3390/fib12110099/s1, Table S1. FTIR absorbance bands for silk conformations; Table S2. Adsorption capacity of silk measured for MB concentration of 150 ppm; Table S3. MB removal data for unraveled plain woven fabrics (PWY); Table S4. Separation factor (R_L); Table S5. Removal efficiencies of PWY for MB concentrations from 5 to 800 ppm; Table S6. Research on silk adsorption capacities; Table S7. Oil adsorption efficiencies of NW for 10 cycles; Figure S1. Optical microscope images of staple and filament silk fibers found in fabrics; Figure S2. Graphical representation of A. preparation of silk fibroin solution and B. synthesis steps for hollow silk microparticle formation and SEM image of the silk particles; Figure S3. FTIR spectra of silk fabrics before and after adsorbing MB dye; Figure S4. UV–visible spectrum depicting MB removal data for PWY; Figure S5. Nonlinear fitting for Q_e vs. C_e data points using, A. Langmuir and B. Freundlich model (respective equations are provided underneath plots); Figure S6. Linear fitting for Q_e vs. C_e data points for concentrations up to 150 ppm.

Author Contributions: Conceptualization, L.M.S. and H.J.; methodology, H.J.; validation, H.J. and I.S.; investigation, H.J. and I.S.; resources, L.M.S.; writing—original draft preparation, H.J.; writing—review and editing, H.J., I.S., and L.M.S.; supervision, L.M.S.; funding acquisition, L.M.S. All authors have read and agreed to the published version of the manuscript.

Funding: This work was performed in part at the Cornell Nanoscale Facility (CNF), a member of the National Nanotechnology Coordinated Infrastructure (NNCI), which is supported by the

National Science Foundation (Grant NNCI-2025233). This work was also partly funded by the AATCC graduate student grants 2024.

Data Availability Statement: Data will be made available upon request.

Acknowledgments: This work made use of the Cornell Center for Materials Research (CCMR) Shared Facilities. The authors acknowledge the following people: CCMR and CNF research staff for training and aid given in using the SEM and Goniometer. The authors are also grateful to Xia (Sam) Zeng for training with various instruments including the UV–visible spectrometer and FTIR. Finally, the authors acknowledge Kyuin Park for the useful input and support given.

Conflicts of Interest: The authors declare no conflicts of interest.

References

1. Rafatullah, M.; Sulaiman, O.; Hashim, R.; Ahmad, A. Adsorption of Methylene Blue on Low-Cost Adsorbents: A Review. *J. Hazard. Mater.* **2010**, *177*, 70–80. [CrossRef] [PubMed]
2. Cláudio Barros, F. Removal of petroleum spill in water by chitin and chitosan. *Orbital-Electron. J. Chem.* **2014**, *39*. [CrossRef]
3. Xiang, B.; Sun, Q.; Zhong, Q.; Mu, P.; Li, J. Current Research Situation and Future Prospect of Superwetting Smart Oil/Water Separation Materials. *J. Mater. Chem. A Mater.* **2022**, *10*, 20190–20217. [CrossRef]
4. Gore, P.M.; Naebe, M.; Wang, X.; Kandasubramanian, B. Progress in Silk Materials for Integrated Water Treatments: Fabrication, Modification and Applications. *Chem. Eng. J.* **2019**, *374*, 437–470. [CrossRef]
5. Belda Marín, C.; Egles, C.; Landoulsi, J.; Guénin, E. Silk Bionanocomposites for Organic Dye Absorption and Degradation. *Appl. Sci.* **2022**, *12*, 9152. [CrossRef]
6. Rastogi, S.; Kandasubramanian, B. Progressive Trends in Heavy Metal Ions and Dyes Adsorption Using Silk Fibroin Composites. *Environ. Sci. Pollut. Res.* **2020**, *27*, 210–237. [CrossRef]
7. Gupta, S.; Kandasubramanian, B. Silk Adsorbent for Green and Efficient Removal of Methylene Blue from Wastewater. *Environ. Sci. Pollut. Res.* **2024**, 1–16. [CrossRef]
8. Martis, L.J.; Parushuram, N.; Sangappa, Y. Preparation, Characterization, and Methylene Blue Dye Adsorption Study of Silk Fibroin–Graphene Oxide Nanocomposites. *Environ. Sci. Adv.* **2022**, *1*, 285–296. [CrossRef]
9. Roberts, A.D.; Lee, J.S.M.; Magaz, A.; Smith, M.W.; Dennis, M.; Scrutton, N.S.; Blaker, J.J. Hierarchically Porous Silk/Activated-Carbon Composite Fibres for Adsorption and Repellence of Volatile Organic Compounds. *Molecules* **2020**, *25*, 1207. [CrossRef]
10. Song, P.; Zhang, D.Y.; Yao, X.H.; Feng, F.; Wu, G.H. Preparation of a Regenerated Silk Fibroin Film and Its Adsorbability to Azo Dyes. *Int. J. Biol. Macromol.* **2017**, *102*, 1066–1072. [CrossRef]
11. Mehdi, M.; Jiang, W.; Zeng, Q.; Thebo, K.H.; Kim, I.S.; Khatri, Z.; Wang, H.; Hu, J.; Zhang, K.Q. Regenerated Silk Nanofibers for Robust and Cyclic Adsorption-Desorption on Anionic Dyes. *Langmuir* **2022**, *38*, 6376–6386. [CrossRef] [PubMed]
12. Shulha, H.; Po Foo, C.W.; Kaplan, D.L.; Tsukruk, V.V. Unfolding the Multi-Length Scale Domain Structure of Silk Fibroin Protein. *Polymer* **2006**, *47*, 5821–5830. [CrossRef]
13. Belbéoch, C.; Lejeune, J.; Vroman, P.; Salaün, F. Silkworm and Spider Silk Electrospinning: A Review. *Environ. Chem. Lett.* **2021**, *19*, 1737–1763. [CrossRef] [PubMed]
14. Nguyen, T.P.; Nguyen, Q.V.; Nguyen, V.H.; Le, T.H.; Huynh, V.Q.N.; Vo, D.V.N.; Trinh, Q.T.; Kim, S.Y.; Van Le, Q. Silk Fibroin-Based Biomaterials for Biomedical Applications: A Review. *Polymers* **2019**, *11*, 1933. [CrossRef]
15. Qi, Y.; Wang, H.; Wei, K.; Yang, Y.; Zheng, R.Y.; Kim, I.S.; Zhang, K.Q. A Review of Structure Construction of Silk Fibroin Biomaterials from Single Structures to Multi-Level Structures. *Int. J. Mol. Sci.* **2017**, *18*, 237. [CrossRef]
16. Wandrekar, S.D. An Unstable Lattice in Silk Fibroin. *Nature* **1938**, *165*, 319–320.
17. Sashina, E.S.; Bochek, A.M.; Novoselov, N.P.; Kirichenko, D.A. Structure and Solubility of Natural Silk Fibroin. *Russ. J. Appl. Chem.* **2006**, *79*, 869–876. [CrossRef]
18. Valluzzi, R.; Gido, S.P.; Zhang, W.; Muller, W.S.; Kaplan, D.L. Trigonal Crystal Structure of Bombyx Mori Silk Incorporating a Threefold Helical Chain Conformation Found at the Air-Water Interface. *Macromolecules* **1996**, *29*, 8606–8614. [CrossRef]
19. Hu, X.; Kaplan, D.; Cebe, P. Determining Beta-Sheet Crystallinity in Fibrous Proteins by Thermal Analysis and Infrared Spectroscopy. *Macromolecules* **2006**, *39*, 6161–6170. [CrossRef]
20. Tretinnikov, O.N.; Tamada, Y. Influence of Casting Temperature on the Near-Surface Structure and Wettability of Cast Silk Fibroin Films. *Langmuir* **2001**, *17*, 7406–7413. [CrossRef]
21. Zhang, X.; Pan, Z. Microstructure Transitions and Dry-Wet Spinnability of Silk Fibroin Protein from Waste Silk Quilt. *Polymers* **2019**, *11*, 1622. [CrossRef] [PubMed]
22. Mukerjee, P.; Kumar Ghosh, A. Thermodynamic Aspects of the Self-Association and Hydrophobic Bonding of Methylene Blue. A Model System for Stacking Interactions. *J. Am. Chem. Soc.* **1963**, *92*, 6419–6424. [CrossRef]
23. Yavari, M.; Salman Tabrizi, N. Adsorption of Methylene Blue from Aqueous Solutions by Silk Cocoon. *Int. J. Eng.* **2016**, *29*, 1191–1197. [CrossRef]
24. Somashekarappa, H.; Annadurai, V.; Subramanya, G.; Somashekar, R. Structure-Property Relation in Varieties of Acid Dye Processed Silk Fibers. *Mater. Lett.* **2002**, *53*, 415–420. [CrossRef]

25. Kalmár, J.; Lente, G.; Fábián, I. Kinetics and Mechanism of the Adsorption of Methylene Blue from Aqueous Solution on the Surface of a Quartz Cuvette by On-Line UV-Vis Spectrophotometry. *Dyes Pigments* **2016**, *127*, 170–178. [CrossRef]
26. Chairat, M.; Rattanaphani, S.; Bremner, J.B.; Rattanaphani, V. An Adsorption and Kinetic Study of Lac Dyeing on Silk. *Dyes Pigments* **2005**, *64*, 231–241. [CrossRef]
27. Mussa, Z.H.; Al-Ameer, L.R.; Al-Qaim, F.F.; Deyab, I.F.; Kamyab, H.; Chelliapan, S. A Comprehensive Review on Adsorption of Methylene Blue Dye Using Leaf Waste as a Bio-Sorbent: Isotherm Adsorption, Kinetics, and Thermodynamics Studies. *Environ. Monit. Assess.* **2023**, *195*, 940. [CrossRef]
28. Wang, J.; Guo, X. Adsorption Isotherm Models: Classification, Physical Meaning, Application and Solving Method. *Chemosphere* **2020**, *258*, 127279. [CrossRef]
29. Tunçeli, A.; Ulaş, A.; Acar, O.; Türker, A.R. Adsorption Isotherms, Kinetic and Thermodynamic Studies on Cadmium and Lead Ions from Water Solutions Using Amberlyst 15 Resin. *Turk. J. Chem.* **2022**, *46*, 193–205. [CrossRef]
30. Huang, W.; Ling, S.; Li, C.; Omenetto, F.G.; Kaplan, D.L. Silkworm Silk-Based Materials and Devices Generated Using Bio-Nanotechnology. *Chem. Soc. Rev.* **2018**, *47*, 6486–6504. [CrossRef]